# Axisymmetric viscous flow between two horizontal plates

Edward M. Hinton[1, a)]

*BP Institute for Multiphase Flow, University of Cambridge, Madingley Road, Cambridge, CB3 0EZ, UK*

(Dated: 4 June 2020)

The flow of viscous fluid injected from a point source into the space between two horizontal plates initially filled with a second fluid of lesser density and different viscosity is studied theoretically and numerically. The volume of the dense input fluid increases with time in proportion to $t^{\alpha}$. When the fluid has spread far from the source, lubrication theory is used to derive the governing equations for the axisymmetric evolution of the interface between the fluids. The flow is driven by the combination of pressure gradients associated with buoyancy and pressure gradients associated with the input flux. The governing equation is integrated numerically and we identify that with a constant input flux, the flow is self-similar at all times with the radius growing in proportion to $t^{1/2}$. In the regimes of injection-dominated and gravity-dominated currents, we obtain asymptotic approximations for the interface shape, which are found to agree well with the numerical computations. For a decreasing input flux ($0 < \alpha < 1$), at short times, the flow is controlled by injection; the current fills the depth of the channel spreading with radius $r \sim t^{\alpha/2}$. At long times, buoyancy dominates and the current becomes unconfined with the radius growing in proportion to $t^{(3\alpha+1)/8}$. The sequence of regimes is reversed in the case of an increasing input flux ($\alpha > 1$) with buoyancy dominating initially while the pressure associated with the injection dominates at late times. Finally, we consider the release of a fixed volume of fluid ($\alpha = 0$). The current slumps under gravity and transitions from confined to unconfined and we obtain asymptotic predictions for the interface shape in both regimes.

a)Electronic mail: edward@bpi.cam.ac.uk

## I. INTRODUCTION

The gravity-driven flow of a viscous fluid occurs in many industrial, environmental and geological settings. In these low Reynolds number gravity currents, viscous stresses play a key role whilst inertial effects may be neglected. In many situations with an injected and an ambient fluid, the problem is simplified because the geometry is 'unconfined'. Examples include shallow flow in a very thick porous medium and the flow of a dense viscous fluid over a rigid boundary[1–4]. The key idea is that the flow of the ambient fluid (for example, air or the host brine in an aquifer) is unimportant and models need consider only the motion of the input fluid. However, in other contexts, the geometry of the flow is 'confined'. Examples include the injection of drilling mud in the wells used for oil and gas extraction and geothermal power[5–7], the storage of $CO_2$ in layered sedimentary deposits[8,9], the evolution of magma chambers[10] and the cleaning of channels[11]. In a confined geometry, the displacement of the ambient fluid, and hence the viscosity ratio between the two fluids, may have a strong influence on the evolution of the flow[12]. Even a single boundary to the flow geometry can alter the scaling laws governing the spreading of a viscous fluid[13].

There has been extensive research on confined displacement flows in pipes with rectangular and circular cross-sections for a wide variety of viscosity ratios in the case of miscible[7,14–16] and immiscible fluids[17–19]. Similar studies have been undertaken for the slumping of one fluid under another in a confined porous medium[3,20–22]. There are many similarities between gravity currents in porous media and viscous gravity currents and in this paper we draw on some of the physical insights provided by previous work focused on porous media (for a more detailed discussion of this analogy, see the review of Huppert[23]).

In the case that viscous fluid is injected into a confined geometry, the flow is driven by the combination of the pressure owing to injection and the buoyancy force whilst it is resisted by viscous stresses and friction at the channel walls. The flow may initially behave as unconfined but as the injected fluid fills the geometry, the displacement of the ambient fluid becomes rate-limiting and there is a transition to confined behavior. Taghavi[24] studied the role of slip at the walls and there has also been investigation of the influence of walls with undulating shape[25,26].

The present paper considers the input of fluid from a point source into the space between two horizontal plates, which is initially filled with a second fluid of lesser density and different viscosity (see figure 1). We assume that inertia is negligible and that the fluids are immiscible. The arising three-dimensional Stokes flow is laterally unconfined and axisymmetric. The transient evolution of the interface between the immiscible fluids is controlled by the viscosity ratio and the relative importance of the buoyancy force and the pressure owing to injection.

The two most similar previous studies are by Zheng *et al.*[12] and Guo *et al.*[27]. The former considered the constant input of viscous fluid into a two-dimensional channel and showed that the flow transitions from being unconfined and buoyancy-dominated to confined and injection-dominated as the channel fills. Guo *et al.* showed that, in the context of a porous medium, if fluid is injected at a constant rate into an axisymmetric geometry, there is no transition between regimes and the evolution is self-similar and confined at all times. Both these studies focus on a constant input flux.

However, in many applications the input flux varies in time or the injection may be periodic[28]. Examples include pumping in biological organisms[29], subsurface fluid injection and extraction[30], and the dynamics of magma chambers[10]. The evolution of the interface is quite different to the constant input flux case and we explore how the flow transitions from unconfined to confined or vice versa, depending on the variation of the input flux.

There has much research on flow in Hele-Shaw cells, which is relevant to the present work. These cells have a very thin gap width and the motion is often approximated as two-dimensional[31]. Experimental and theoretical analysis of the transverse structure of the flow in the case of miscible fluids has shown that the gap-averaged concentration profile has growing rarefaction regions and shock-like regions[32–34]. We obtain similar behavior for an immiscible displacement in at thicker channel in the regime where the flow is dominated by the input flux.

The no-slip flow condition at the top and bottom boundaries leads to a parabolic velocity profile, with fluid in the center of the channel travelling fastest. It is possible for a dense input fluid to predominantly migrate through the center of the channel and over-ride a finger of lighter fluid at the bottom boundary[35]. However, a sufficient density difference between the two fluids ensures that the dense fluid lies underneath the lighter fluid (and hence the interface remains monotonic) and we assume this is the case herein[1].

It is well-known that a fingering instability may occur when a less viscous fluid displaces a more viscous fluid in a Hele-Shaw cell[31]. There has been extensive study on how such an instability may be controlled and even suppressed by various physical ingredients including surface tension[36], channel geometry[37] and the injection rate[38,39]. In the case that the effects of surface tension are negligible, the wavelength of fingers is proportional to the thickness of the cell into which fluid is injected[40]. The density difference between the injected and ambient fluids may also play a key role in suppressing the viscous instability. Laboratory experiments by Pegler *et al.*[8] showed that in a confined porous medium, the viscous instability has a negligible effect on the global behavior of the current owing to the stabilizing influence of the hydrostatic pressure. In an unconfined two-layer viscous gravity current, a sufficiently large density difference between the fluids may suppress the viscous instability[41]. Henceforth, we neglect viscous fingering effects but note that they may play an important role if the density difference is small or if the input fluid is of much lower viscosity than the ambient. It is worth noting that the present analysis could be used as a base state for a study investigating the stability of the interface to viscous fingering. For example, in the case of unconfined two-layer viscous gravity currents, the flow was found experimentally to be unstable for particular viscosity ratios (Kowal and Worster[42]), which motivated a perturbation study of the base state to analyze the origin of the instability[41,43]. Other examples where the base state has been used to inform stability calculations include the fingering that occurs in inclined viscous gravity currents[44] and the work of Mathunjwa and Hogg[45], which demonstrated the linear stability of the similarity solution for porous gravity currents above a horizontal impermeable boundary.

The paper is structured as follows. In section II, the governing equations for the evolution of the interface between the two fluids is derived in the case that the volume increases as a power-law function of time. We assume that inertia is negligible and that the pressure within the fluids is hydrostatic. We identify a function of time that quantifies the importance of the input flux relative to the buoyancy force. In section III, we introduce a numerical method for the governing equations and present some results. These suggest that the flow is self-similar at all times in the case of constant input flux and that there is a transition between confined and unconfined in the case of a power-law varying volume. To provide insight into the influence of the physical ingredients of confinement, injection, buoyancy and the viscosity ratio, we seek simplified asymptotic solutions to the governing equations. In section IV, we obtain a similarity solution for the case of constant input flux, which is accurate at all times. We approximate this solution in the regimes of injection-dominated flow and buoyancy-dominated flow and show how the accuracy of our approximations depends on the viscosity ratio.

In section V, we consider input fluxes that vary in time. In the case that the input flux increases, the flow evolves in a self-similar fashion at early times when it is unconfined and buoyancy-dominated. At late times, the flow is confined and there is an injection-dominated similarity solution. For a decreasing input flux, the situation is reversed, with the flow initially confined.

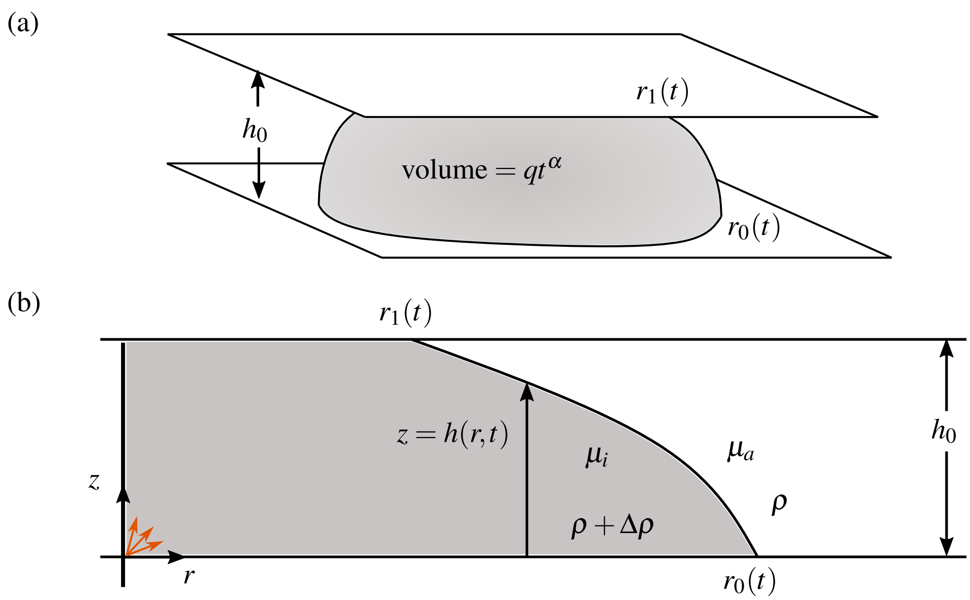


FIG. 1. (a) Schematic for the injection of viscous fluid between two horizontal plates. (b) Radial cross-section. The origin ($r = 0$, $z = 0$) is located at the input source.

We then consider the finite release of a fixed volume of fluid in section VI. The flow is always buoyancy-dominated but transitions between confined and unconfined as it slumps. We investigate the influence of the initial shape of the release on this behavior. In section VII, the results of the paper are summarized and we discuss some important applications.

## II. MODEL

The problem of interest concerns the flow of viscous fluid in the gap between two rigid horizontal plates. We consider the injection of liquid of density $\rho + \Delta\rho$ and viscosity $\mu_i$ from a point source located on the lower plate. The impermeable plates are separated by a finite distance $h_0$ and the space is initially occupied by a second fluid of lesser density $\rho$ and viscosity $\mu_a$ (figure 1). The flow is axisymmetric because the channel is isotropic and hence we use cylindrical coordinates $(r,z)$ with $r = 0$ corresponding to the location of the source. We assume that the fluids are immiscible and we neglect surface tension. We denote the depth of the injected fluid by $z = h(r,t)$. In this paper, the viscous limit is taken; inertial forces are negligible in comparison to the viscous stresses. For an incompressible Newtonian fluid, the fluid motion can then be described by the creeping-flow equations[46],

$$\mu_i \nabla^2 \mathbf{u}_i - \nabla p + (\rho + \Delta\rho)\mathbf{g} = 0, \qquad \nabla \cdot \mathbf{u}_i = 0, \tag{1}$$

$$\mu_a \nabla^2 \mathbf{u}_a - \nabla p + \rho \mathbf{g} = 0, \qquad \nabla \cdot \mathbf{u}_a = 0, \tag{2}$$

in the injected and ambient fluids, respectively. Once the invading fluid has spread beyond a horizontal distance $l \gg h_0$ from the source, the flow is predominantly in the radial direction and the lubrication approximation may be applied. At early times, the shape of the fluid-fluid interface may not have a small aspect ratio (see figure 2). However, at later times, the current becomes long ($l \gg h_0$) and the flow in the near-source region where vertical velocities may be significant has a negligible influence on the global dynamics[1,13]. In this paper, we include some early-time results that have large aspect ratios because they help illustrate the dynamics of the flow. In the following sections, we discuss the relevance of our lubrication model at early times in more detail. We show that, provided the parameter $\Lambda$ satisfies particular conditions, each of the early-time regimes observed in figure 2 may occur with a small aspect ratio so that the lubrication approximation is self-consistent.

When the vertical velocity is negligible, the pressure adopts a hydrostatic distribution given by the following expressions

$$p_i(r,z,t) = p_0 - (\rho + \Delta\rho) g z \qquad \text{for} \quad 0 \le z \le h, \tag{3}$$

$$p_a(r,z,t) = p_0 - \rho g z - \Delta\rho g h \qquad \text{for} \quad h \le z \le h_0, \tag{4}$$

for the injected and ambient fluids respectively, where $p_0 = p_0(r,t)$ is the unknown pressure on the lower boundary ($z = 0$). The Stokes equations (1), (2) are simplified by applying the lubrication approximation to obtain[47]

$$\frac{\partial p_i}{\partial r} = \mu_i \frac{\partial^2 u_i}{\partial z^2}, \tag{5}$$

$$\frac{\partial p_a}{\partial r} = \mu_a \frac{\partial^2 u_a}{\partial z^2}, \tag{6}$$

where $u_i(r,t)$ and $u_a(r,t)$ denote the radial velocities of the injected and ambient fluids, respectively. The boundary conditions for the velocities are no-slip at the top and bottom boundaries,

$$u_i = u_a = 0, \quad \text{at} \quad z = 0, h_0 \tag{7}$$

and continuity of velocity and tangential stress across the interface between the two fluids,

$$\left.\begin{aligned} u_i &= u_a, \\ \mu_i \tfrac{\partial u_i}{\partial z} &= \mu_a \tfrac{\partial u_a}{\partial z} \end{aligned}\right\} \quad \text{at } z = h(r,t). \tag{8}$$

Since the pressure gradients (equations 3 and 4) are independent of $z$ we can integrate equations (5) and (6) twice and apply the four boundary conditions for the velocities (7, 8) to obtain

$$u_i(r,z,t) = \frac{p_{i,r}}{2\mu_i}\left(z^2 - \frac{[2Mh_0 + (1-2M)h]h_0 p_{i,r} + M(h_0-h)^2 p_{a,r}}{[h+M(h_0-h)]p_{i,r}} z\right) \tag{9}$$

$$\begin{aligned} u_a(r,z,t) = \frac{p_{a,r}}{2\mu_a}\Bigg(& z^2 + \frac{h^2 p_{i,r} - [Mh_0^2 - (M-2)h^2]p_{a,r}}{[h+M(h_0-h)]p_{a,r}} z \\ & - \frac{h_0 h^2 p_{i,r} + h_0 h[(1-M)h_0 + (M-2)h]p_{a,r}}{[h+M(h_0-h)]p_{a,r}}\Bigg), \end{aligned} \tag{10}$$

where $p_{i,r} = \partial p_i/\partial r$, $p_{a,r} = \partial p_a/\partial r$ are the pressure gradients and

$$M = \mu_i/\mu_a \tag{11}$$

is the viscosity ratio. We consider the range $0.01 \leq M \leq 100$. In this paper, capital letters are used to denote dimensionless quantities and lower-case letters for dimensional quantities.

To close the problem, we must determine the unknown pressure gradients, $\partial p_i/\partial r$ and $\partial p_a/\partial r$. We differentiate equation (3) and equation (4) with respect to $r$ and then subtract the first from the second to obtain the following equation relating the two pressure gradients,

$$\Delta\rho g \frac{\partial h}{\partial r} = p_{i,r} - p_{a,r}. \tag{12}$$

Mass conservation provides a second relation. Injection begins at $t = 0$. We consider sources of fluid of strength such that the volume of fluid injected is

$$\int_0^{r_0(t)} 2\pi r h\, dr = qt^{\alpha} \tag{13}$$

where $\alpha \geq 0$ and $r_0(t)$ is the leading contact point of the current; $h(r_0(t),t) = 0$ (figure 1). Mass conservation of the injectate (13) can be recast as a condition on the total flux across the channel (for $r > 0$),

$$\int_0^h u_i\, dz + \int_h^{h_0} u_a\, dz = \frac{\alpha q t^{\alpha-1}}{2\pi r}. \tag{14}$$

We substitute the expressions for the radial velocities (9), (10) into this flux condition to obtain a second equation relating the pressure gradients, $p_{a,r}$, and $p_{i,r}$. This relation is solved together with equation (12) to obtain the following expressions for the pressure gradients,

$$\begin{aligned} p_{i,r} = &-\frac{12[h+M(h_0-h)]\mu_i}{b(M,h_0,h)}\frac{\alpha q t^{\alpha-1}}{2\pi r}, \\ &+\frac{[h^2-M(h_0-h)^2]^2-h^4+Mh(4h_0+h)(h_0-h)^2}{b(M,h_0,h)}\Delta\rho g\frac{\partial h}{\partial r} \end{aligned} \tag{15}$$

$$p_{a,r} = p_{i,r}+\Delta\rho g\frac{\partial h}{\partial r}, \tag{16}$$

where

$$b(M,h_0,h) = [h^2-M(h_0-h)^2]^2+4Mh_0^2h(h_0-h). \tag{17}$$

We use these relations to obtain the equation governing the evolution of the flow depth. Local mass conservation for the injected fluid takes the form

$$r\frac{\partial h}{\partial t} = -\frac{\partial}{\partial r}\left(r\int_0^{h(r,t)} u_i(r,z,t)\,dz\right). \tag{18}$$

We use our expression for the velocity of the injectate, $u_i$ (9), and the pressure gradients, (3) and (4), to transform equation (18) into an advection-diffusion type equation for the depth of the current, $z=h(r,t)$,

$$\begin{aligned} r\frac{\partial h}{\partial t}+\frac{\alpha q t^{\alpha-1}}{2\pi}\frac{\partial}{\partial r}\left(\frac{h^2(3Mh_0^2+h[(1-M)h-2Mh_0])}{b(M,h_0,h)}\right) = \\ \frac{\Delta\rho g}{3\mu_i}\frac{\partial}{\partial r}\left(\frac{Mrh^3(h_0-h)^3((1-M)h+Mh_0)}{b(M,h_0,h)}\frac{\partial h}{\partial r}\right). \end{aligned} \tag{19}$$

To complete the mathematical description, we require initial and boundary conditions. Injection begins at $t=0$ so

$$h(r,0)=0. \tag{20}$$

At the contact point along the lower plate, $r=r_0(t)$, the boundary condition is

$$h(r_0(t),t)=0. \tag{21}$$

To calculate the boundary condition at $r = 0$, we first differentiate the mass conservation equation (13) with respect to time. Then applying (21), we obtain

$$\int_0^{r_0(t)} 2\pi r \frac{\partial h}{\partial t}\, dr = \alpha q t^{\alpha-1}. \tag{22}$$

By integrating the governing equation (19) between $r = 0$ and $r = r_0(t)$ and applying (21) and (22), we obtain the boundary condition at $r = 0$,

$$\left[\frac{\alpha q t^{\alpha-1}}{2\pi}\frac{h^2(3Mh_0^2 + h[(1-M)h - 2Mh_0])}{b(M,h_0,h)} - \frac{\Delta\rho g}{3\mu_i}\frac{Mrh^3(h_0-h)^3((1-M)h + Mh_0)}{b(M,h_0,h)}\frac{\partial h}{\partial r}\right]_{r=0} = \frac{\alpha q t^{\alpha-1}}{2\pi}. \tag{23}$$

## A. Non-dimensionalization

We scale the horizontal and vertical coordinates with the depth of the channel, $h_0$. We use the timescale

$$t_0 = \frac{3\mu_i}{\Delta\rho g h_0}, \tag{24}$$

which is the timescale for a gravity-driven viscous fluid to propagate a distance $h_0$. It is independent of the input flux. We introduce the following dimensionless variables

$$H = h/h_0, \qquad R = r/h_0, \qquad T = t/t_0. \tag{25}$$

The dimensionless form of equation (19) is given by

$$R\frac{\partial H}{\partial T} + \Lambda T^{\alpha-1}\frac{\partial}{\partial R}\left(\frac{H^2\{3M + H[(1-M)H - 2M]\}}{B(M,H)}\right) = \frac{\partial}{\partial R}\left(\frac{MRH^3(1-H)^3[(1-M)H + M]}{B(M,H)}\frac{\partial H}{\partial R}\right), \tag{26}$$

where

$$\Lambda = \frac{\alpha q t_0^{\alpha}}{2\pi h_0^3} \tag{27}$$

and

$$B(M,H) = [H^2 - M(1-H)^2]^2 + 4MH(1-H). \tag{28}$$

Note that in the case of equally viscous fluids ($M = 1$), this reduces to $B(1,H) = 1$. The right-hand side of (26) is a diffusive term that arises from gradients of the hydrostatic pressure associated with buoyancy forces whilst the second term on the left-hand side is advective and is associated with the injection. The parameter $\Lambda$ represents the dimensionless volume of fluid injected in the time interval $[0,t_0]$, where $t_0$ is the gravity-driven timescale. The prefactor $\Lambda T^{\alpha-1}$ quantifies the relative significance of injection, it is the ratio of the input flux, $\alpha q t^{\alpha-1}$ to the flux associated with buoyancy, $2\pi h_0^3/t_0$. In the special case of constant input flux ($\alpha = 1$), this ratio is equal to $\Lambda$ and is independent of time. For $\alpha \neq 1$, the relative significance of injection and buoyancy is time-dependent because the input flux varies.

The dimensionless form of the mass conservation condition (13) is given by

$$\int_0^{R_0(T)} RH\,dR = \frac{\Lambda T^\alpha}{\alpha}, \tag{29}$$

where $R_0(T) = r_0(t)/h_0$ is the position of the leading contact point. Fluid input begins at $t = 0$, which yields the following initial condition

$$H(R,0) = 0. \tag{30}$$

The boundary condition at the leading contact point is given by

$$H(R_0(T),T) = 0. \tag{31}$$

The dimensionless boundary condition at $R = 0$ is obtained from its dimensional analogue (23),

$$\left[\Lambda T^{\alpha-1}\frac{H^2\{3M + H[(1-M)H - 2M]\}}{B(M,H)} - \frac{MRH^3(1-H)^3[(1-M)H + M]}{B(M,H)}\frac{\partial H}{\partial r}\right]_{R=0} = \Lambda T^{\alpha-1}, \tag{32}$$

which is associated with mass conservation (29). When the channel is flooded fully by the input fluid, this boundary condition reduces to $H(R=0,T) = 1$. We note that in the fully-flooded region in which $H = 1$, we recover Poiseuille flow with dimensionless velocity given by

$$U_i = \frac{6\Lambda T^{\alpha-1}}{R}(1-Z)Z. \tag{33}$$

We next illustrate some aspects of the flow in the injected and ambient fluids in the interface region where $0 < H < 1$. The dimensionless fluxes in the two fluids in the case of equal viscosities ($M = 1$) is obtained from (9), (10), (15), (16),

$$Q_i = \int_0^H U_i\,dZ = \frac{\Lambda T^{\alpha-1} H^2(3-2H)}{R} - H^3(1-H)^3\frac{\partial H}{\partial R}, \tag{34}$$
$$Q_a = \int_H^1 U_a\,dZ = \frac{\Lambda T^{\alpha-1}(1-H)^2(1+2H)}{R} + H^3(1-H)^3\frac{\partial H}{\partial R}. \tag{35}$$

The first term in the fluxes arises from the injection, whilst the second term is associated with buoyancy. In the injected fluid, both terms are positive (since $\partial H/\partial R < 0$). In the ambient fluid, the flux associated with injection acts outwards but buoyancy acts in the opposite direction. The flux in the ambient fluid is towards the source if

$$\frac{\Lambda T^{\alpha-1}}{R}(1+2H) < H^3(1-H)\left(-\frac{\partial H}{\partial R}\right), \tag{36}$$

for equally viscous fluids ($M = 1$). We note that in the case of zero injection ($\Lambda = 0$), the flux in the ambient fluid is always towards the source.

## III. NUMERICAL RESULTS

The advection-diffusion equation (26) with boundary conditions (31), and (32), and initial condition (30) was integrated numerically using the finite difference scheme of Kurganov and Tadmor[48], for details see Appendix A of Zheng *et al.*[49]. The results for a constant input flux ($\alpha = 1$), an increasing input flux ($\alpha = 2$), and a decreasing input flux ($\alpha = 1/2$) are shown in the three panels of figure 2, from early to late times. In figure 2, the parameter values used are $\Lambda = 1$ and $M = 1$ to illustrate the time evolution for different values of the exponent $\alpha$.

Figure 2a shows that for a constant input flux ($\alpha = 1$), the solution is self-similar at all times with the radius growing as $R \sim T^{1/2}$. In this case, the ratio of the advective and diffusive terms in equation (26) is a constant, $\Lambda$. Thus, the importance of injection relative to gravity-driven slumping is independent of time. In section IV, we study how the self-similar interface shape is controlled by the magnitude of $\Lambda$ and the viscosity ratio $M$ in the case of constant input flux.

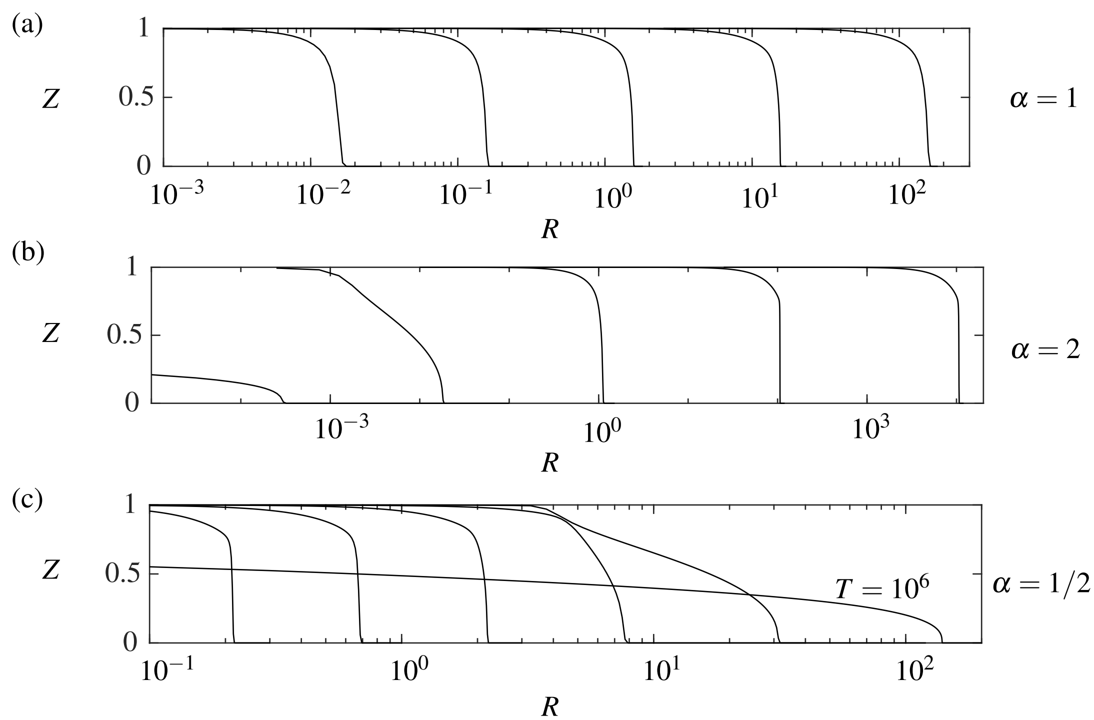


FIG. 2. Thickness of the injected current in a confined axisymmetric channel for: (a) a constant input flux ($\alpha = 1$), (b) an increasing input flux ($\alpha = 2$), and (c) a decreasing input flux ($\alpha = 1/2$). The results are calculated numerically as described in §III with $\Lambda = 1$ and $M = 1$. The interface is shown at $T = 10^{-4}$, $10^{-2}$, 1, $10^2$, and $10^4$, and in (c) the extra solution at $T = 10^6$ is included to illustrate the transition to an unconfined current. (a) The solution is self-similar at all times with $R \sim T^{1/2}$ and $H \sim 1$. (b) At early times the flow is unconfined with $R \sim T^{(3\alpha+1)/8} = T^{7/8}$ and $H \sim T^{(\alpha-1)/4} = T^{1/4} \ll 1$. As the input flux increases with time the current transitions to a late-time similarity solution with $R \sim T^{\alpha/2} = T$ and $H \sim 1$. In (c), the situation is reversed because the input flux decreases with time and the current transitions from confined at early times with $R \sim T^{\alpha/2} = T^{1/4}$ and $H \sim 1$ to unconfined with $R \sim T^{(3\alpha+1)/8} = T^{5/16}$ and $H \sim T^{(\alpha-1)/4} = T^{-1/8} \ll 1$ at late times.

For an increasing or decreasing input flux, the importance of the gravity-driven slumping relative to the pressure associated with injection is time-dependent. In the case of increasing input flux, the advective term in equation (26) grows in time; at early times the diffusive slumping dominates and at late times injection dominates. This is illustrated in figure 2b. The dominance of the slumping leads to a thin, unconfined current at early times. As the input flux increases, the depth of the current grows until it transitions to a confined flow primarily driven by injection. The dynamics are reversed for the case of decreasing input flux (see figure 2c). We study these regimes in detail in section V and we find similarity solutions in the injection-driven and buoyancy-driven limits. Although, the early time interface shapes may not satisfy the lubrication approximation, they are included because they assist in understanding the dominant physics associated with the governing equations and illustrate how the flow transitions from injection-driven to buoyancy-driven or vice versa.

## IV. CONSTANT INPUT FLUX ($\alpha = 1$)

In the special but important case of a constant rate of injection, the relative significance of the advective and diffusive terms in equation (26) is time-invariant; both terms scale with $R^{-1}$. The full governing equations have an exact similarity solution with $R^2 \sim T$ which we obtain below. We then study the regimes in which the force associated with the constant input flux is large (§IV B) or small (§IV C) relative to gravity, corresponding to $\Lambda \gg 1$ and $\Lambda \ll 1$, respectively. In both regimes, we obtain asymptotic predictions for the shape of the interface that agree well with the numerical results (see figure 3).

### A. Similarity solution

The interfaces in figure 2a indicate that in the case of a constant input flux the interface shape is self-similar at all times with $R \sim T^{1/2}$. This scaling may be obtained by inspecting the terms in equation (26). The second term on the left-hand side and the term on the right-hand side both scale as $\mathscr{O}(R^{-1})$, and balancing these terms with the time derivative leads to $R \sim T^{1/2}$. The scaling is also associated with mass conservation (29) because the volume of the current ($V \sim R^2$) increases in proportion to $\Lambda T$.

This observation motivates introducing the similarity variable $\eta = R^2/(\Lambda T)$ and writing $H(R,T) = \Upsilon(\eta)$. Equation (26) can be recast in terms of $\eta$ and $\Upsilon$

$$-\eta \frac{\mathrm{d}\Upsilon}{\mathrm{d}\eta} + 2\frac{\mathrm{d}}{\mathrm{d}\eta}\left(\frac{\Upsilon^2(3M + \Upsilon[(1-M)\Upsilon - 2M])}{B(M,\Upsilon)}\right) = 4\Lambda^{-1}\frac{\mathrm{d}}{\mathrm{d}\eta}\left(\frac{M\eta\Upsilon^3(1-\Upsilon)^3((1-M)\Upsilon + M)}{B(M,\Upsilon)}\frac{\mathrm{d}\Upsilon}{\mathrm{d}\eta}\right). \quad (37)$$

(a)

(b)

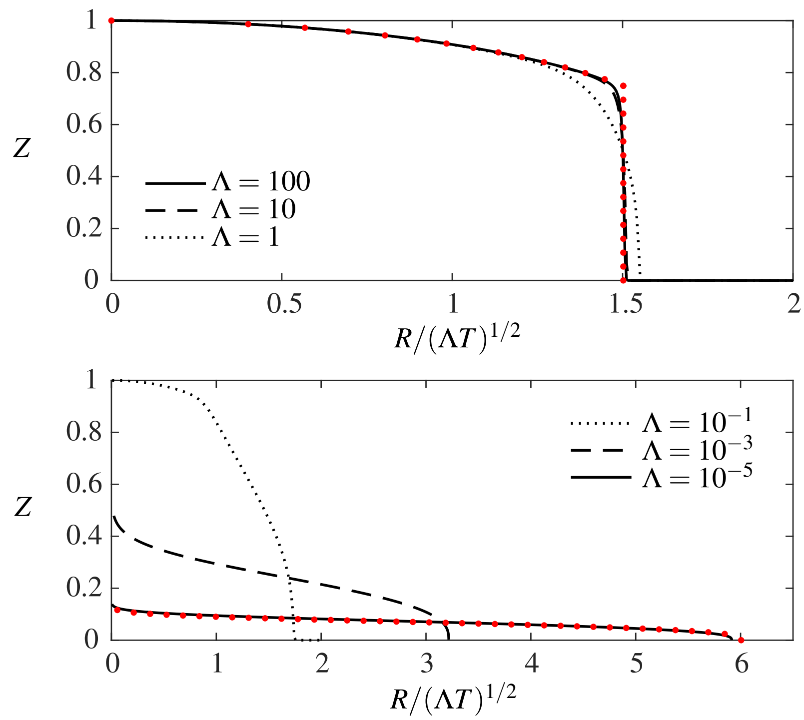


FIG. 3. The thickness of the injected current in the case of constant input flux ($\alpha = 1$) and equally viscous fluids ($M = 1$) in terms of the similarity coordinate, $R/(\Lambda T)^{1/2}$. The numerical results are plotted as black lines. (a) For a relatively high input flux ($\Lambda \gg 1$), the interface shape is well-approximated by the asymptotic prediction (red dotted line) of §IV B for which the diffusive term is neglected. (b) For a relatively low input flux ($\Lambda \ll 1$), the current occupies a thin region of the channel and buoyancy dominates. The asymptotic prediction of §IV C shows excellent agreement with the numerical result for $\Lambda = 10^{-5}$. Note that for $\Lambda \ll 1$, the asymptotic solution in these coordinates depends on $\Lambda$.

The boundary condition at the leading contact point (equation 31) becomes

$$\Upsilon(\eta_0) = 0, \tag{38}$$

where $\eta_0 = R_0(T)^2/(\Lambda T)$ is a constant representing the position of the leading contact point in the similarity coordinate. To solve equation (37) numerically, a second boundary condition at $\eta = \eta_0$ is required, which we determine by letting $\Upsilon \to 0$ to obtain the leading order behavior near $\eta_0$,

$$\Upsilon = \left[\frac{3\Lambda(\eta_0 - \eta)}{4}\right]^{1/3}, \qquad \frac{\mathrm{d}\Upsilon}{\mathrm{d}\eta} = -\frac{\Lambda}{4}\left[\frac{3\Lambda(\eta_0 - \eta)}{4}\right]^{-2/3}. \tag{39}$$

The unknown position of the contact point $\eta_0$ is determined with an iterative shooting scheme using the mass conservation constraint (29) in terms of the similarity coordinate,

$$\int_0^{\eta_0} \Upsilon(\eta)\mathrm{d}\eta = 2. \tag{40}$$

The numerical solutions to the system (37, 39, 40) agree with the finite-difference integration of the full governing equations at all times. This is because the system is self-similar at all times. In particular, the similarity solution is an exact solution for arbitrarily small times because the initial condition $H(R,0) = 0$ is in the solution space of the self-similar form of the governing equations. Thus, $H(R,T)$ is identically equal to $\Upsilon(\eta)$ at all times. Guo *et al.*[27] found the same result for constant input flux into a confined axisymmetric porous medium. There is no transition period in the case of constant input flux because the relative importance of the advective and diffusive terms is constant.

We note that although the similarity solution is an exact solution to the formulated governing equations at all times, the model predicts that the current has not spread far from the input point at early times. Thus the lubrication approximation is violated at early times. However, the similarity solution does apply to the physical problem at later times when the injectate has spread further. The extent of the current is $R \sim T^{1/2}$ and its thickness is independent of time, $H \sim 1$. The lubrication approximation applies when $R/H = r/h \gg 1$, so we find that the model is valid for $T \gg 1$, provided that $\Lambda$ is of order unity. In the regimes of large and small $\Lambda$, the dimensionless time, $T$, at which the lubrication approximation applies depends on $\Lambda$, which we discuss below.

In the next two subsections, we find approximate solutions in the regimes of $\Lambda \gg 1$ and $\Lambda \ll 1$ by neglecting the diffusive or advective term, respectively. The resultant simplified equations and their solutions provide insight into the physics governing the flow by isolating one of the key physical ingredients: pressure owing to injection or gravity-driven slumping. In addition, the approximations enable the influence of the viscosity ratio on the motion to be determined. Figure 3a shows how the interface shape behaves in the regime $\Lambda \gg 1$. Figure 3b shows the behavior for $\Lambda \ll 1$. In each panel, the red dots show our asymptotic approximations and the black lines are obtained from the numerical method.

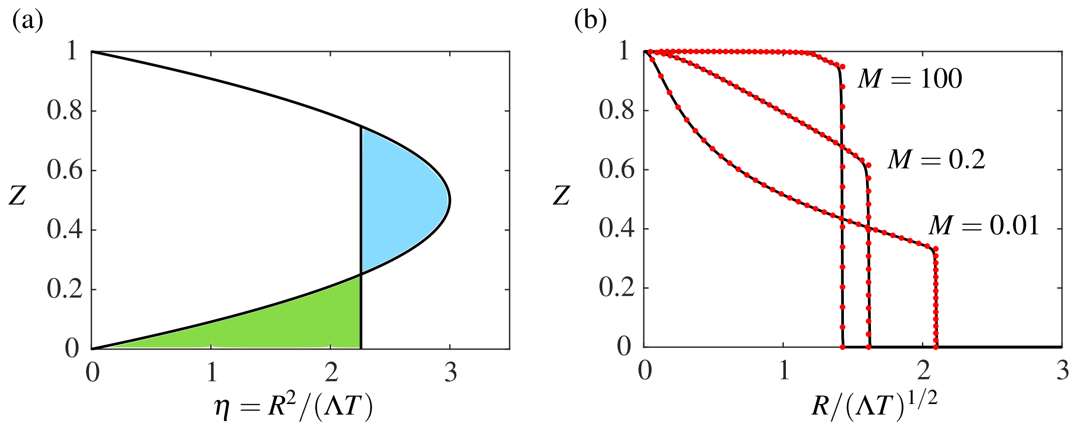


FIG. 4. Evolution of the interface in the case that the pressure associated with injection dominates ($\Lambda \gg 1$). (a) Illustration of the 'equal area' rule. The position of the shock (vertical line) is chosen so that the green area equals the blue area, which corresponds to mass conservation (40). (b) The shape of the interface according to the numerical solutions to equation (37) with $\Lambda = 100$ for three values of the viscosity ratio, $M$ (black lines). There is excellent agreement with the $\Lambda \gg 1$ asymptotic prediction (equation 46, red dots) for which the term associated with gravity-driven slumping is neglected.

### B. Injection-dominated regime ($\Lambda \gg 1$)

In the regime $\Lambda \gg 1$, the flow is dominated by injection and the role of the gravity-driven slumping of the injectate is negligible. This motivates the following approximate equation

$$R\frac{\partial H}{\partial T} + \Lambda\frac{\partial}{\partial R}\left(\frac{H^2(3M + H[(1-M)H - 2M])}{B(M,H)}\right) = 0, \tag{41}$$

where the diffusive term in (26) has been neglected. In terms of the similarity coordinates, $\eta = R^2/T$ and $\Upsilon(\eta) = H(R,T)$, this can be rewritten as

$$\left(-\eta + 2\frac{\mathrm{d}F}{\mathrm{d}\Upsilon}\right)\frac{\mathrm{d}\Upsilon}{\mathrm{d}\eta} = 0, \tag{42}$$

where

$$F(\Upsilon) = \frac{\Upsilon^2\{3M + \Upsilon[(1-M)\Upsilon - 2M]\}}{B(M,\Upsilon)}, \tag{43}$$

is the flux function. Given that $d\Upsilon/d\eta = 0$ leads to a trivial solution, equation (42) becomes

$$\eta = 2\frac{\mathrm{d}F}{\mathrm{d}\Upsilon}. \tag{44}$$

For isoviscous fluids ($M = 1$), this reduces to

$$\eta = 12\Upsilon(1-\Upsilon), \tag{45}$$

from which we observe that the depth, $\Upsilon(\eta)$, is multivalued. This solution is associated with heavy injectate lying above less dense ambient fluid (the blue area in figure 4a). Such behavior is inconsistent with the derivation of the governing equations in section II where we assumed that the sharp interface is a single-valued function of radial distance. The interface shape (45) corresponds to the case in which the two fluids have the same density because the term associated with buoyancy has been neglected. The solution is identical to a pressure-driven Poiseuille flow in which the flow speed is fastest in the center of the channel and decays to 0 at the top and bottom boundaries owing to the viscous drag there. In the case that the input fluid is more dense, we anticipate that buoyancy forces drive the injectate in the middle of the channel down towards the bottom boundary[50].

To overcome the multivalued behavior, we seek a weak solution (with a discontinuity). There is a shock across the lower part of the channel, whose location is determined by mass conservation (40) and continuity of the interface. This is illustrated in figure 4a; the vertical shock is positioned so that the blue region and the green region have equal areas. In the case $M = 1$, the shock position, $\eta_s = 9/4$ and magnitude, $\Upsilon_s = 3/4$ can be obtained analytically. When $M \neq 1$, the shock position is found using an iterative procedure in which the blue and green areas are calculated numerically. Mathematically, the shock arises because the flux function $F(\Upsilon)$ is neither concave nor convex, and the characteristics of the first-order equation (41) cross in $\Upsilon < \Upsilon_s$. The solution cannot be determined here and a weak solution must be sought[51].

The interface shape is given by

$$\eta = \begin{cases} \eta_s & 0 \leq \Upsilon \leq \Upsilon_s \\ 2\frac{\mathrm{d}F}{\mathrm{d}\Upsilon} & \Upsilon_s < \Upsilon \leq 1. \end{cases} \tag{46}$$

There is a region of fixed extent and a region that grows in time. Figure 4b shows these compound rarefaction-shock solutions as red dots for three values of the viscosity ratio, $M$. The numerical results for $\Lambda = 100$ (black lines) show good agreement with the asymptotic solutions. For a lower viscosity ratio ($M$) the shock height is reduced and the current has greater lateral extent. A current of relatively lower viscosity runs further along the base of the channel because this requires displacing less of the viscous ambient fluid which provides resistance to flow. Similar dynamics occur in the case of injection into a confined porous medium[8,9].

Finally, we calculate the time at which lubrication theory is applicable. The extent of the current is $R_0 \sim (\Lambda T)^{1/2}$ and the thickness is $H \sim 1$ so the ratio, $R/H$ is large at times satisfying $T \gg \Lambda^{-1}$.

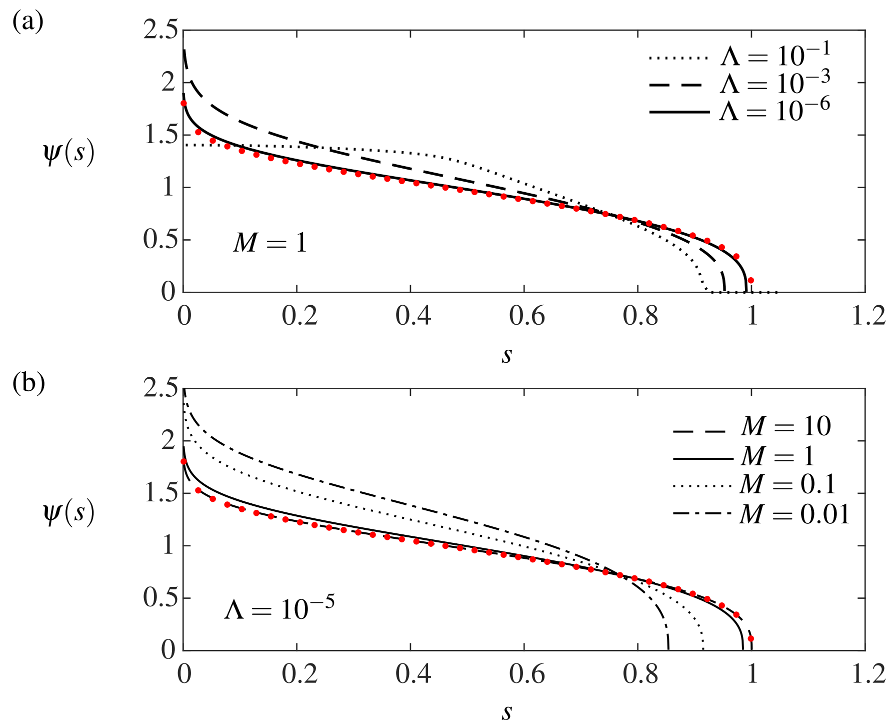


FIG. 5. Evolution of the interface in the buoyancy-dominated regime, in scaled similarity coordinates. The asymptotic solution for small $\Lambda$, found in section IV C, is shown in red dots. (a) The numerical results for isoviscous fluids and three values of $\Lambda$. There is excellent agreement for $\Lambda = 10^{-6}$. (b) The effect of the viscosity ratio in the case that $\Lambda = 10^{-5}$. The accuracy of the asymptotic solution increases strongly with $M$ up to $M \sim 1$.

### C. Buoyancy-dominated regime ($\Lambda \ll 1$)

In this section, we seek a simplified analytic solution in the case that buoyancy dominates ($\Lambda \ll 1$).

The flow is controlled primarily by the gravity-driven slumping of the injectate. We neglect the term associated with the pressure owing to injection in equation (26), which yields the approximate equation

$$R\frac{\partial H}{\partial T} = \frac{\partial}{\partial R}\left(\frac{MRH^3(1-H)^3((1-M)H+M)}{B(M,H)}\frac{\partial H}{\partial R}\right). \tag{47}$$

The numerical solutions in figure 3b demonstrate that in the limit $\Lambda \ll 1$, the current occupies a thin region at the base of the channel. This motivates linearizing (47) in $H$, taking $H \ll 1$ and $|(1-M)H| \ll M$, which correspond to the regime of a thin and unconfined current for which the motion of the ambient fluid has a negligible influence on the evolution of the injectate. By applying these approximations to equation (47), we obtain

$$R\frac{\partial H}{\partial T}=\frac{\partial}{\partial R}\left(RH^3\frac{\partial H}{\partial R}\right). \tag{48}$$

Note that the viscosity ratio, $M$ is absent from this equation, which is as expected for unconfined flows. The diffusion equation (48) has been previously studied by Huppert[1] who derived it as the governing equation in the case of viscous flow over a rigid horizontal boundary for a power-law varying volume. He found that equation (48) together with mass conservation (29) and the boundary condition at the leading edge (31) admits a self-similar solution, which we outline below for the special case of constant input flux.

The input flux is constant and so the scalings are as before: $R\sim T^{1/2}$ and $H$ is a function of $R/T^{1/2}$ only. To balance the terms in equation (48) and eliminate $\Lambda$ from the mass conservation equation (29), we use the following variables

$$\zeta=\Lambda^{-3/8}RT^{-1/2}, \quad \text{and} \quad H=\zeta_0^{2/3}\Lambda^{1/4}\psi(s), \tag{49}$$

where $s=\zeta/\zeta_0=R/R_0(T)$. The constant $\zeta_0$ and the shape function, $\psi(s)$ are to be determined. The diffusion equation (48) is recast as

$$2(s\psi^3\psi')'+s^2\psi'=0, \tag{50}$$

with $\psi(1)=0$. Mass conservation can be rearranged to obtain the following expression for the contact point

$$\zeta_0=\left(\int_0^1 s\psi(s)\mathrm{d}s\right)^{-3/8}. \tag{51}$$

Equation (50) is second order and requires a second boundary condition. Letting $s\to 1^-$ and $\psi\to 0$, gives the following leading order behavior

$$\psi(s)=(3/2)^{1/3}(1-s)^{1/3}, \qquad \psi'(s)=-18^{-1/3}(1-s)^{-2/3}, \tag{52}$$

which provides the two boundary conditions near $s=1$. Equation (50) is solved numerically with these boundary conditions and we find that $\zeta_0\approx 1.424$. The front location is given by

$$\eta_0=R_0^2/(\Lambda T)=\zeta_0^2\Lambda^{-1/4}. \tag{53}$$

The shape, $\psi(s)$, is plotted with red dots in figure 5. The numerical solutions to the full governing equations are also plotted in the $s$, $\psi(s)$ coordinates. Figure 5a, in which $M=1$, demonstrates

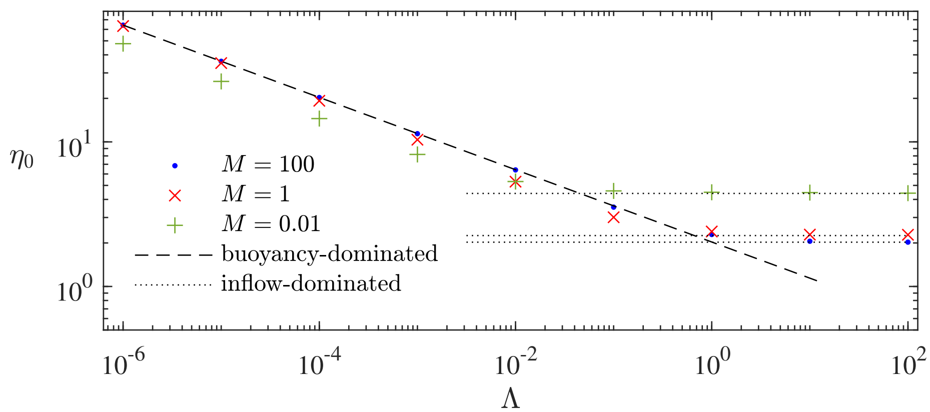


FIG. 6. The position of the leading contact point, $\eta_0 = R_0^2/(\Lambda T)$, as a function of the parameter $\Lambda$ for three values of the viscosity ratio, $M$ in the case of constant input flux ($\alpha = 1$). The scatter points represent numerical results. In the regime $\Lambda \gg 1$, injection dominates and the location of the contact point depends only on $M$ as discussed in §IV B. The asymptotic predictions in this regime are shown as dotted lines. In the regime $\Lambda \ll 1$, buoyancy dominates and the asymptotic prediction of §IV C, $\eta_0 = \zeta_0^2 \Lambda^{-1/4}$ is plotted as a dashed line. The agreement improves with increasing $M$ up to $M \sim 1$ as discussed in the text.

that the agreement between the similarity solution and the full numerical results improves with smaller $\Lambda$, as expected. However, the comparison suggests that $\Lambda$ must be very much less than 1 for the asymptotic solution to be a good approximation. The agreement also depends on the viscosity ratio, $M$, as shown in figure 5b, where $\Lambda = 10^{-5}$. The agreement improves with larger $M$ up to about $M \sim 1$. We investigate how the accuracy of the $\Lambda \ll 1$ asymptotic solution as an approximation depends on the parameters $\Lambda$ and $M$ more formally below.

The scalings (49) suggest that the current thickness scales as $H \sim \Lambda^{1/4}$. The approximate equation (48) assumed the flow is unconfined and in particular $H \ll 1$ and $|(1-M)H| \ll M$. For $M \ll 1$, these conditions are equivalent to $\Lambda \ll M^4$, whilst for $M \gg 1$, the corresponding condition is $\Lambda \ll 1$. Therefore, the agreement between the numerical results and the similarity solution increases with $M$ up until $M \sim 1$, whilst the agreement improves weakly with decreasing $\Lambda$ since $H \sim \Lambda^{1/4}$. The dependence of these conditions on the viscosity ratio can be interpreted physically as follows. In the case that the input fluid is of relatively very low viscosity ($M \ll 1$), the accuracy of the similarity solution is limited by the assumption that the displacement of the ambient fluid is unimportant. Thus, the agreement is improved with a less adverse viscosity ratio. In the case that the input fluid is much more viscous than the ambient, the displacement of the ambient fluid is less significant and the agreement is limited predominantly by the requirement that the current is thin. Hence for $M \gg 1$, the agreement is insensitive to increases in the viscosity ratio, $M$.

The results of this section are summarized in figure 6, which shows the location of the contact point in similarity coordinates, $\eta_0 = R_0^2/(\Lambda T)$, as a function of the parameter $\Lambda$ for three values of the viscosity ratio, $M$. The numerical results are shown as scatter points, whilst the asymptotic predictions for injection- and buoyancy-dominated evolution are shown as dotted and dashed lines, respectively. There is excellent agreement between the numerical results and asymptotic predictions in the relevant regimes.

The time at which lubrication theory is applicable is different for the present case of $\Lambda \ll 1$ from the previous section. The extent of the current is $R_0 \sim \Lambda^{3/8} T^{1/2}$ and the thickness is $H \sim \Lambda^{1/4}$ so the ratio, $R/H$ is large at times satisfying $T \gg \Lambda^{-1/4}$.

## V. INCREASING OR DECREASING INPUT FLUX ($\alpha \neq 1$)

In the present section we consider input fluxes that vary in time such that the volume of fluid is given by a power-law function of time (equation 29). In the case where the input flux decreases in time ($\alpha < 1$), the flow is confined and dominated by the pressure associated with injection at early times whilst at late times, the gravity-driven slumping of the fluid dominates and the current is unconfined. In the case of an increasing input flux ($\alpha > 1$), the situation is reversed (see figure 2). This behavior contrasts with the case of a constant input flux ($\alpha = 1$) for which the relative importance of injection and gravity is independent of time but controlled by the parameter $\Lambda$, as described in the previous section.

To study the varying input flux case, we first note that when $\alpha \neq 1$, the independent variables, $T$ and $R$, may be rescaled to remove $\Lambda$ from equation (26) with

$$\tilde{T} = \Lambda^{1/(\alpha-1)} T, \qquad \tilde{R} = \Lambda^{1/2(\alpha-1)} R. \tag{54}$$

The governing equations are recast as

$$\tilde{R}\frac{\partial H}{\partial \tilde{T}} + \tilde{T}^{\alpha-1}\frac{\partial}{\partial \tilde{R}}\left(\frac{H^2(3M+H[(1-M)H-2M])}{B(M,H)}\right) = \frac{\partial}{\partial \tilde{R}}\left(\frac{M\tilde{R}H^3(1-H)^3((1-M)H+M)}{B(M,H)}\frac{\partial H}{\partial \tilde{R}}\right) \tag{55}$$

and

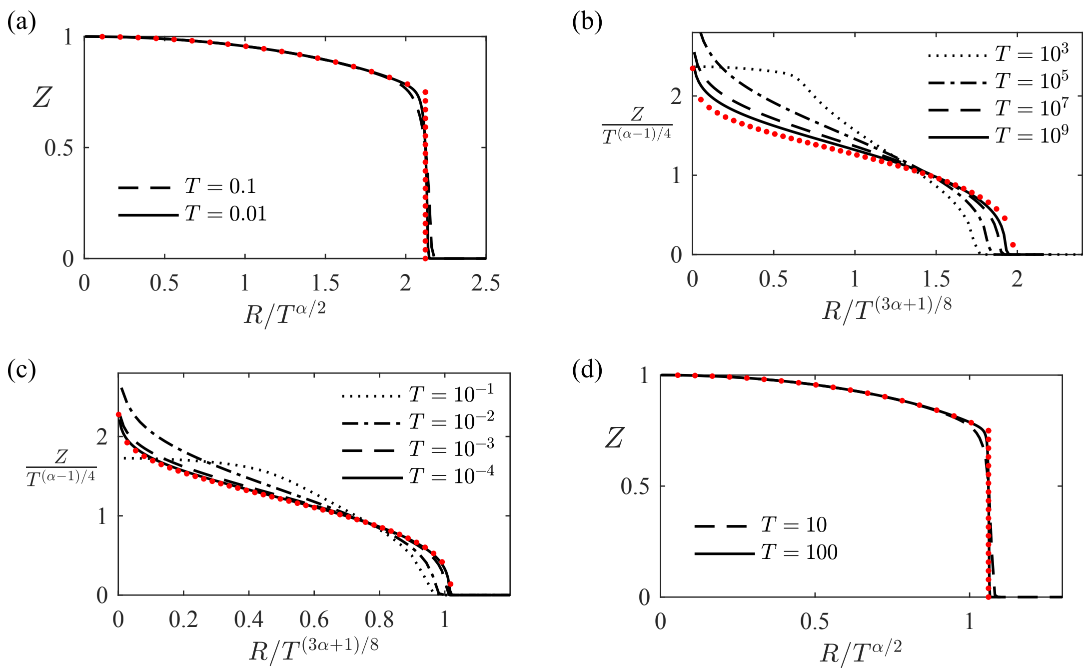


FIG. 7. Interface evolution for a varying input flux with $\Lambda = 1$ and $M = 1$. In (a) and (b), the input flux decreases with time ($\alpha = 1/2$). In (c) and (d), the input flux increases with time ($\alpha = 2$). The injection-dominated similarity solution of section V A is shown as red dots in (a) and (d). The flow is dominated by the pressure owing to injection at early times when $\alpha < 1$ and at late times when $\alpha > 1$. Similarly, in (b) and (c) the gravity-dominated solution of section V B is shown as red dots. The flow is dominated by the gravity-driven slumping at late times when $\alpha < 1$ and at early times when $\alpha > 1$.

$$\int_0^{\tilde{R}_0} \tilde{R} H \mathrm{d}\tilde{R} = \frac{\tilde{T}^\alpha}{\alpha}, \tag{56}$$

which is equivalent to the original governing equations but with tilde variables and $\Lambda = 1$. Thus, solutions to the original governing equations may be found for any value of $\Lambda$ by solving in the case $\Lambda = 1$ and then rescaling $R$ and $T$ as necessary. Therefore, in this section, we restrict our attention to $\Lambda = 1$ (and drop tildes). The rescaling (54) also has implications for the relevance of the lubrication approximation. The early-time regimes for $\alpha \neq 1$ do not have a small aspect ratio in the case $\Lambda = 1$ (see figure 2b and figure 2c) but these early regimes can occur with a small aspect ratio if $\Lambda \ll 1$ and $\alpha > 1$ or if $\Lambda \gg 1$ and $\alpha < 1$ since $\Lambda \neq 1$ corresponds to rescaling the radial coordinate.

## A. Injection-dominated regime

In the present section, we obtain a similarity solution for the current evolution in the case that injection dominates and the flow is confined. This similarity solution is valid at early times in the case of a decreasing input flux and late times in the case of an increasing input flux. It is a generalization of the injection-dominated behavior that occurs for a constant input flux (§IV B). The rate at which fluid is injected is proportional to $T^{\alpha-1}$ and the advective term in the governing equation has the same scaling. For a decreasing input flux ($\alpha < 1$), this term is large at early times and for an increasing input flux ($\alpha > 1$), this term is large at late times. In both cases we anticipate that the term on the right-hand side of equation (55) is negligible in comparison to the second term on the left-hand side. We neglect the contribution from buoyancy in the governing equation and obtain

$$R\frac{\partial H}{\partial T} + T^{\alpha-1}\frac{\partial}{\partial R}\left(\frac{H^2(3M+H[(1-M)H-2M])}{B(M,H)}\right) = 0. \tag{57}$$

Figure 2 suggests that the current is confined and the channel is fully-flooded in this regime and hence $H \sim 1$. Then balancing the two terms in (57) and using mass conservation motivates the similarity variables, $\chi = \alpha R^2/T^\alpha$ and $H(R,T) = \Theta(\chi)$. These transform equation (57) to

$$\left(-\chi + 2\frac{\mathrm{d}F}{\mathrm{d}\Theta}\right)\frac{\mathrm{d}\Theta}{\mathrm{d}\chi} = 0 \tag{58}$$

where $F(H)$ is given by equation (43). As in section IV B, the solution is

$$\chi = 2\frac{\mathrm{d}F}{\mathrm{d}\Theta}. \tag{59}$$

To find the position of the shock, we use the equal area rule, with mass conservation given by

$$\int_0^{\chi_0} \Theta(\chi)\mathrm{d}\chi = 2. \tag{60}$$

where $\chi_0 = \alpha R_0(T)^2/T^\alpha$ is a constant corresponding to the contact point. Equation (59) and mass conservation (60) are the same as those found for constant input flux in section IV B and hence the interface shapes in terms of the similarity variable, $\chi$, are identical to those in figure 4b, which illustrates the role of $M$.

The numerical solutions to the full governing equations for early times and $\alpha = 1/2$, and late times and $\alpha = 2$ show good agreement with the asymptotic solution in figure 7a and 7d with $M = 1$.

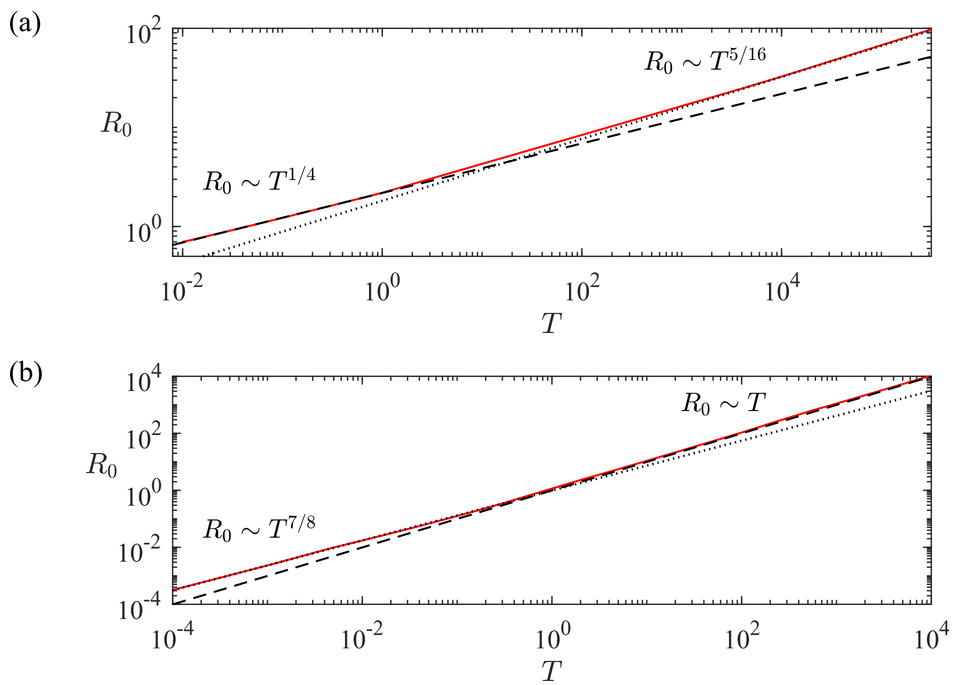


FIG. 8. Location of the leading contact point of the current, $R_0$, as a function of time in the case (a) $\alpha = 1/2$, a decreasing input flux and (b) $\alpha = 2$, an increasing input flux. In both cases, $M = 1$ and $\Lambda = 1$. The numerical result is plotted as a continuous red line. The buoyancy-dominated behavior for which $R_0 \sim T^{(3\alpha+1)/8}$ is plotted as black dotted line, whilst the injection-dominated behavior for which $R_0 \sim T^{\alpha/2}$ is plotted as a black dashed line. For $\alpha = 1/2$, the evolution transitions from injection-dominated to buoyancy-dominated and for $\alpha = 2$ the sequence is reversed.

### B. Buoyancy-dominated regime

In the previous section we showed that the similarity solution at early times for $\alpha < 1$ has the same form as the similarity solution at late times for $\alpha > 1$. In the present section, we consider the other regime in which buoyancy dominates which corresponds to late times when the input flux is decreasing ($\alpha < 1$) and early times when the input flux is increasing ($\alpha > 1$). These regimes are demonstrated in figure 2b and figure 2c.

Buoyancy forces dominate when there is a relatively low input flux. The current occupies a thin region above the lower plate and the flow is approximately unconfined. This situation corresponds to the buoyancy dominated regime for constant input flux (see figure 3b). We therefore follow similar analysis to section IV C and first neglect the term associated with the pressure owing to injection and assume $H \ll 1$, which yields

$$R\frac{\partial H}{\partial T} = \frac{\partial}{\partial R}\left(RH^3\frac{\partial H}{\partial R}\right). \tag{61}$$

The similarity solution in the case of constant input flux (equation 49) can be generalized to account for a power-law volume[1]

$$\zeta = \alpha^{3/8}R/T^{(3\alpha+1)/8}, \quad H = \zeta_0^{2/3}\alpha^{-1/4}T^{(\alpha-1)/4}\phi(s), \tag{62}$$

where $s = \zeta/\zeta_0 = R/R_0(T)$, $\zeta_0$ corresponds to the contact point, and $\phi(s)$ is the shape function which satisfies

$$(s\phi^3\phi')' + \tfrac{1}{8}(3\alpha+1)s^2\phi' - \tfrac{1}{4}(\alpha-1)s\phi = 0, \tag{63}$$

with $\phi(1) = 0$. Mass conservation (29), with $\Lambda = 1$, can be used to find the contact point

$$\zeta_0 = \left(\int_0^1 s\phi(s)\mathrm{d}s\right)^{-3/8}. \tag{64}$$

The ODE (63) is second order and requires a second boundary condition. We let $s \to 1^-$ in (63) to find the leading order behavior near the contact point,

$$\phi(s) = \left[\frac{3}{8}(3\alpha+1)\right]^{1/3}(1-s)^{1/3}, \tag{65}$$

which provides the boundary conditions for the numerical procedure. The shape which arises is plotted as red dots in figure 7b for $\alpha = 1/2$, and in figure 7c for $\alpha = 2$. These asymptotic results are compared to the full numerical solution at four different times.

Finally, we determine a relationship between the parameters and the dimensionless time, $T$ at which each regime occurs. The injection-dominated regime described in the previous subsection occurs when $\Lambda T^{\alpha-1} \gg 1$. For the present analysis to apply and buoyancy to dominate requires $\Lambda T^{\alpha-1} \ll \min(1, M^4)$, which is obtained by following the argument at the end of section IV C. These two relationships are valid for any value of the exponent $\alpha$. To illustrate the regime transitions, the location of the leading contact point is plotted in figure 8, as a function of time in the case that $\alpha = 1/2$ and $\alpha = 2$. The numerical results (continuous red line) are compared to the predictions of the similarity solutions for injection-dominated and buoyancy-dominated flow.

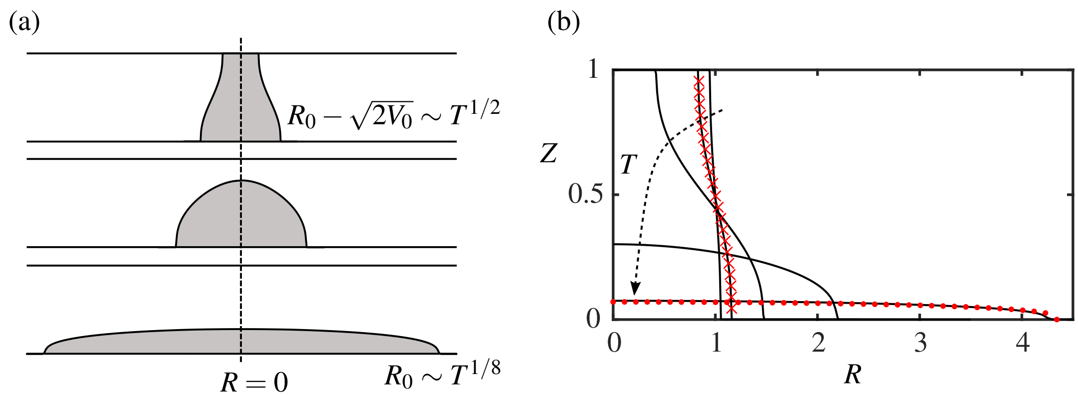


FIG. 9. (a) Schematic for the slumping of a fixed-volume release of fluid in a confined axisymmetric channel. The scaling for the position of the contact point at early and late times is included. (b) Evolution of the fluid-fluid interface in the case of equally viscous fluids with $V_0 = 1/2$. Numerical solutions at $T = 0.1$, 1, 10, $10^2$ and $10^4$ are plotted in black. The confined asymptotic solution at $T = 1$ is shown as red crosses, and the unconfined solution at $T = 10^4$ as red dots.

## VI. RELEASE OF A FIXED VOLUME ($\alpha = 0$, $\Lambda = 0$)

In the present section, we consider the special case in which there is no ongoing injection of fluid. Instead, a fixed volume of the dense fluid is released at $t = 0$.

So far in this paper we have focused on two regimes: (i) a confined current for which the flow is driven predominantly by the pressure owing to injection and (ii) an unconfined current which is primarily driven by gravity-driven slumping. In the present section, where we consider the instantaneous release of a fixed volume of fluid, gravity-driven slumping always dominates and there are two different asymptotic regimes: confined gravity-driven flow and unconfined gravity-driven flow. Provided the depth of the initial volume of fluid is comparable to the size of the gap between the plates, the flow is confined at early times and the motion of the ambient fluid is important. At later times, the released volume has slumped significantly under its own weight, becoming much shallower than the channel (see figure 9a). The influence of the motion of the ambient fluid on the current becomes negligible and the flow behaves as if it were unconfined. This is analogous to regime (ii) described earlier in the paper. We study these two regimes in turn.

In the case of an instantaneous release of fluid, the dimensional quantity $q$ represents the initial volume released. We use the same non-dimensionalization as before (25) because the timescale was defined by the buoyancy velocity. The volume exponent is $\alpha = 0$ and $\Lambda = 0$. Mass conserva-

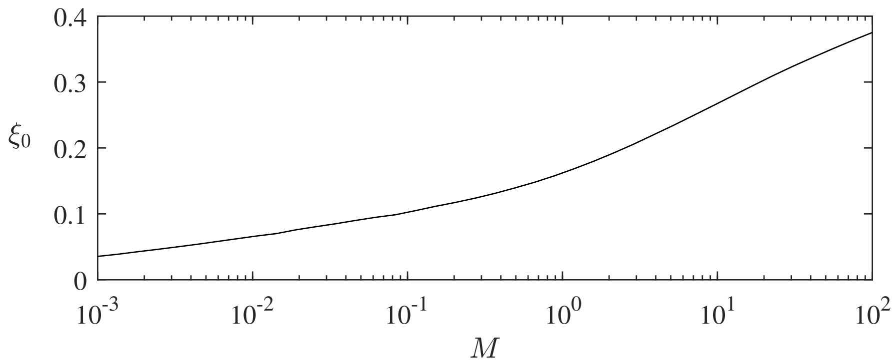


FIG. 10. Position of the leading contact point in similarity coordinates, $\xi = \xi_0$, as a function of the viscosity ratio, $M$.

tion in the dimensionless variables is

$$\int_0^{R_0(t)} RH\mathrm{d}R = V_0, \tag{66}$$

where $V_0 = q/(2\pi h_0^3)$ is the dimensionless volume released. The governing equation can be obtained from (26) by setting $\Lambda = 0$,

$$R\frac{\partial H}{\partial T} = \frac{\partial}{\partial R}\left(\frac{MRH^3(1-H)^3((1-M)H+M)}{B(M,H)}\frac{\partial H}{\partial R}\right). \tag{67}$$

Since there is no ongoing injection, the boundary condition at $R = 0$ may be obtained by considering symmetry,

$$\left(\frac{\partial H}{\partial R}\right)_{R=0} = 0. \tag{68}$$

## A. Early times

We first consider the release of a cylinder of fluid, centered about the $Z$ axis, spanning the thickness of the channel. In dimensionless variables, the initial condition has height of 1, volume $V_0$, and hence radius $R = \sqrt{2V_0}$ (see equation 66).

At short times after release, the radius of the slumping fluid is close to its initial value. This motivates using the coordinate, $\hat{R} = R - \sqrt{2V_0}$, where $\hat{R} \ll \sqrt{2V_0}$. The governing equation may be approximated by

$$\frac{\partial H}{\partial T} = \frac{\partial}{\partial \hat{R}}\left(\frac{MH^3(1-H)^3((1-M)H+M)}{B(M,H)}\frac{\partial H}{\partial \hat{R}}\right). \tag{69}$$

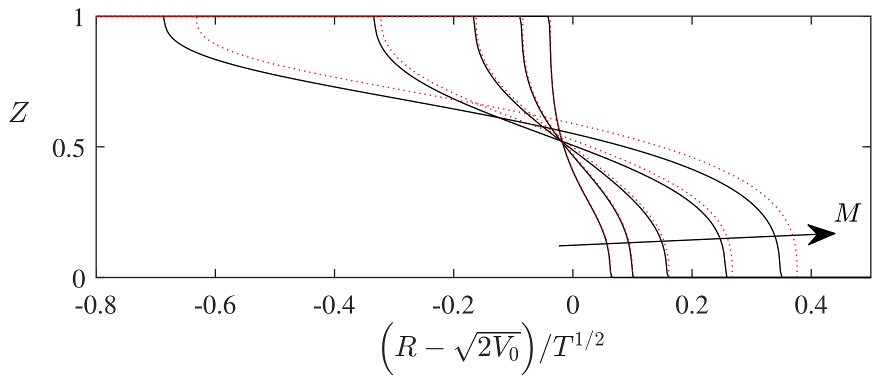


FIG. 11. Shape of the interface between the fluids as a function of the similarity variable $\xi = \left(R - \sqrt{2V_0}\right)/T^{1/2}$ at time $T = 20$ with $V_0 = 10$ for $M = 0.01, 0.1, 1, 10, 100$. The numerical solution to the governing equations is plotted as a continuous black line and compared to the early-time similarity solution (red dashed line) of §VI A. The agreement is excellent for small values of the viscosity ratio, $M$, but declines for large $M$. The solution for large $M$ corresponds to the solution for small $M$ but at later times as described by the symmetry (70).

We note that this equation is identical to that for the slumping of viscous fluid in a two-dimensional confined channel with $\hat{R}$ representing the lateral coordinate[12]. Equation (69) is invariant under the following transformation[21]

$$M_1 = M^{-1} \quad \hat{R}_1 = -\hat{R} \quad H_1 = 1 - H \quad T_1 = T/M, \tag{70}$$

which corresponds to a swapping of the fluids in the two-dimensional problem and the change in $T$ arises because the timescale (24) is defined in terms of the viscosity of the released fluid. Equation (69) is self-similar and we transform it using the variable, $\xi = \hat{R}/T^{1/2}$, to obtain the following ordinary differential equation,

$$-\frac{\xi}{2}\frac{\mathrm{d}H}{\mathrm{d}\xi} = \frac{\mathrm{d}}{\mathrm{d}\xi}\left(\frac{MH^3(1-H)^3((1-M)H+M)}{B(M,H)}\frac{\mathrm{d}H}{\mathrm{d}\xi}\right). \tag{71}$$

At early times, the current remains attached to the lower boundary at $R = R_0(T)$ and the upper boundary at $R = R_1(T)$ and in the similarity coordinate, we label these points as $\xi_0$ and $\xi_1$, respectively. The boundary condition at the contact point, $\xi = \xi_0$ can be determined by letting $H \to 0$ to obtain the leading order behavior for small $H$,

$$H = (3\xi_0/2)^{1/3}(\xi_0 - \xi)^{1/3} \tag{72}$$

For each value of $M$, the solution to (71) is obtained by a shooting method. We begin with the case $M = 1$. An initial guess is made of $\xi_0 = 0.01$ and then (71) is integrated numerically from $H = 0$ using the behavior (72) to provide two boundary conditions there. The limit of $H$ as $\xi \to -\infty$ is 0.078. The value of $\xi_0$ is increased and the method repeated until the limit of $H$ as $\xi \to -\infty$ is first equal to 1. We obtain $\xi_0 = 0.1611$ in the case of isoviscous fluids. The value of $\xi_0$ as a function of $M$ is shown in figure 10.

Our early-time similarity solution is valid provided that the perturbation to the initial interface is small, i.e. $\hat{R} \sim T^{1/2} \ll (2V_0)^{1/2}$. Hence the similarity solution is a good approximation for $T \ll 2V_0$. In figure 11, the early-time similarity solution (red dashed lines) is compared to the numerical results at $T = 20$ with $V_0 = 10$ (continuous black lines) for five values of the viscosity ratio, $M$. The agreement is excellent for small $M$. However, the agreement is weaker for larger $M$. This can be interpreted in light of the symmetry (70). The interface shape for large $M$ at $T = 20$ is identical to the shape for a viscosity ratio of $M^{-1}$ at time $T = 20M$, which is much later. At such large times, the radius is not well approximated by a perturbation to its initial value of $R = \sqrt{2V_0}$.

The lubrication approximation is valid provided that the lateral extent of the interface is much greater than the channel thickness, which corresponds to $\hat{R} \sim T^{1/2} \gg 1$. Since we also require that $\hat{R} \ll (2V_0)^{1/2}$ for the early-time similarity solution to be a good approximation, self-consistency imposes $V_0 \gg 1$ in order for this early solution to occur in the physical problem.

At much later times the current detaches from the upper boundary and subsequently occupies a progressively thinner region of the channel. This behavior is described in subsection VI C. In the next subsection, we consider the release of a current that does not initially fully flood the channel.

### B. Partially filled initial conditions

We consider the release of a cylindrical volume with a dimensionless radius of $\sqrt{2V_0}$ but thickness given by $0 < Z < H_i$, where $H_i < 1$. The dimensionless volume is thus $H_iV_0$. We note that the early-time interface shape is still governed by the similarity scaling from the previous section with $\hat{R} \sim T^{1/2}$ (see figure 12). To determine the similarity solution, we shoot numerically in equation (71) from $\xi = \xi_0$ towards $\xi = 0$. The boundary condition at $H = 0$, $\xi = \xi_0$ is given by (72). We repeat the shooting procedure and vary $\xi_0$ until we obtain $H \to H_i$ in the far field. For example, with $H_i = 0.8$, and $M = 1$, we find $\xi_0 = 0.14725$ (see figure 12).

At later times, the depth at the wall slumps away from its initial value, and the interface shape

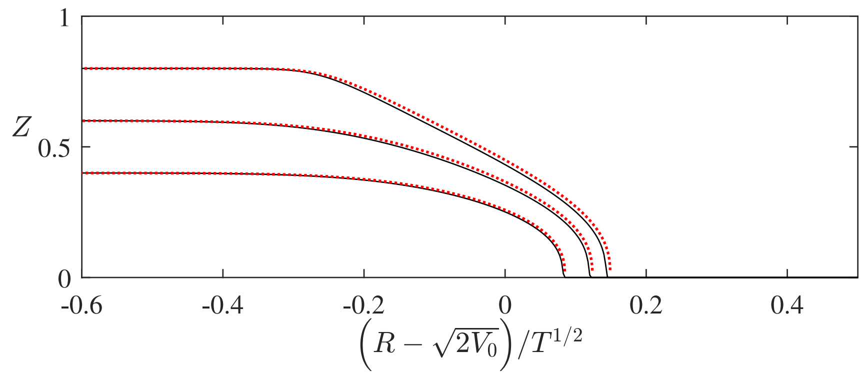


FIG. 12. The interface shape in the case of a partially filled initial condition in the case of equally viscous fluids ($M=1$) at $T=20$ with $V_0=10$ for three values of the initial current height, $H_i=0.4, 0.6, 0.8$. The numerical result (black line) is compared to the early-time similarity solution (red dashed line).

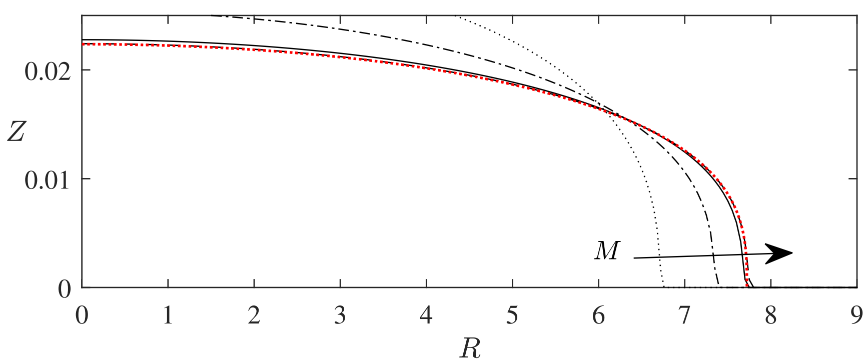


FIG. 13. The interface shapes at $T=10^6$ with $V_0=1/2$ for four values of the viscosity ratio, $M=0.01, 0.1, 1, 10$ calculated numerically (black lines). There is good agreement with the similarity solution (red dotted line, equation 74) for $M=1, 10$.

stops being self-similar.

## C. Late times

At late times, the current becomes progressively thinner as the fluids slumps owing to its own weight. This motivates applying the unconfined approximation of sections IV C and V B. The governing equation is approximated by

$$R\frac{\partial H}{\partial T}=\frac{\partial}{\partial R}\left(RH^3\frac{\partial H}{\partial R}\right). \tag{73}$$

The system has the following self-similar solution[1,52]

$$H = V_0^{1/4} \frac{2^{13/12}}{3^{1/3}} T^{-1/4} \Psi(s) \tag{74}$$

where

$$\Psi(s) = (3/16)^{1/3}(1-s^2)^{1/3}, \qquad s = 2^{-13/8} 3^{1/2} V_0^{-3/8} R T^{-1/8}. \tag{75}$$

The position of the contact point is given by $s = 1$, which corresponds to

$$R_0(T) = 2^{13/8} 3^{-1/2} V_0^{3/8} T^{1/8}. \tag{76}$$

The initial volume is $V_0$ for a cylindrical initial release with $H_i = 1$. The solution is plotted in figure 9 (red dots) for $V_0 = 1/2$ and there is good agreement with the late-time numerical solution in the case of equally viscous fluids, $M = 1$. Figure 13 shows the numerical solutions at $T = 10^6$ for $M = 0.01, 0.1, 1, 10$ compared to the similarity solution (74). As in the previous buoyancy-dominated, unconfined regimes, the agreement improves strongly with increasing $M$ up to $M \sim 1$. We also note that the lubrication approximation is satisfied provided that $R/H \gg 1$, which corresponds to $T \gg V_0^{-1/3}$.

In figure 14, the transition from early- to late-time behavior discussed in the present section is shown. The location of the leading contact point, $R_0$, is plotted as a function of time, $T$ in the case of equally viscous fluids ($M = 1$) and $V_0 = 1/2$. The transition between the confined and unconfined regimes occurs at approximately $T \sim 10^2$ in this case.

## VII. DISCUSSION AND CONCLUSION

We have analyzed the injection and release of a viscous fluid into an axisymmetric channel, which contains a relatively buoyant ambient fluid of different viscosity. Previous work on this problem has studied the constant input of fluid into a two-dimensional channel[12] and the constant input of fluid into a porous medium[8,9,27]. The present paper is novel in two key ways. First, we have considered two-phase viscous flow in a three-dimensional axisymmetric channel. Second, in addition to the case of a constant input flux, the effect of varying rates of input flux and the instantaneous release of fluid have been studied. In this section we summarize our results and discuss some applications.

The two-phase flow of viscous fluid in a vertically confined axisymmetric channel is governed by the relative magnitude of the slumping owing to gravity and the pressure associated with injection. With a fixed input flux, the ratio of these two effects is a constant, $\Lambda$. The structure of

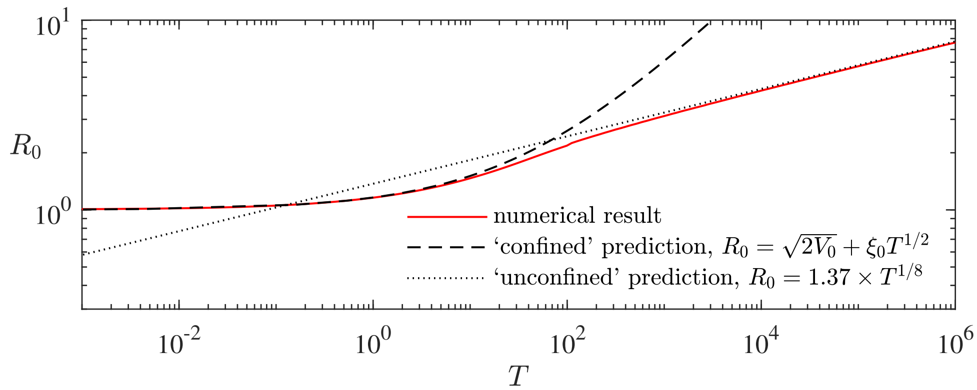


FIG. 14. Location of the leading contact point, $R_0$, as a function of time in the case of an instantaneous release of fluid with $M = 1$ and $V_0 = 1/2$. At early times, the confined approximation of section VI A applies and $R_0 - \sqrt{2V_0} \sim T^{1/2}$. At late times ($T$ larger than about $10^3$) the current becomes unconfined (the motion of the ambient fluid is unimportant) and $R_0 \sim T^{1/8}$, where the constant is given by equation (76). The interface shapes are shown in figure 9.

the flow is self-similar at all times and depends only on $\Lambda$ and the viscosity ratio, $M$. We have determined asymptotic solutions in the case that injection dominates ($\Lambda \gg 1$) and in the case that the flow is thin and dominated by gravity ($\Lambda \ll 1$). Our solutions agree with numerical integrations of the governing equations. We have also obtained relationships between the parameters for which each regime occurs demonstrating that the accuracy of the unconfined approximation is highly sensitive to the viscosity ratio when the input fluid is of lower viscosity than the ambient. When the input flux varies as a power-law function of time, the relative importance of the two processes varies in time and we have generalized our results to this case. The flow structure transitions from gravity-driven to injection-driven in the case of increasing input flux and vice-versa in the case of a decreasing input flux.

In the case that a fixed volume of fluid is released, the flow is driven by gravity and we have shown that it transitions from a confined current that fills the aquifer to an effectively unconfined current occupying a thin region at the base of the channel. In the former case, the displacement of the ambient fluid is important and we derive an asymptotic solution that quantifies the role of the viscosity ratio. When the flow is unconfined, the behavior is analogous to the buoyancy-dominated regimes in the case of non-zero input flux.

To demonstrate the relevance of our results, we describe two applications and calculate in which regime the behavior lies. In the manufacture of toothpaste, many surfaces and channels have to be cleaned[11]. One approach is to inject a viscous fluid to displace the fouling deposit. A typical input fluid has viscosity of 100 Pa s and the density difference, $\Delta\rho$ is of order 100 kgm$^{-3}$. The displaced deposit also has a viscosity of approximately 100 Pa s and hence the viscosity ratio is $M \approx 1$. With these parameter values, in a channel of thickness $h_0 = 2$ cm, the timescale for gravity-driven viscous slumping is $t_0 = 15$ seconds. For a constant input flux of 0.01 m$^3$s$^{-1}$, we calculate that $\Lambda = 3\times10^3$ and hence injection dominates. Also, the lubrication approximation applies when $R_0 \sim (\Lambda T)^{1/2} \gg 1$, which corresponds to times much greater than five milliseconds.

We next consider a magma chamber of thickness $h_0 = 10^3$ metres in which a finite volume of magma slumps under the ambient magma which is relatively hotter and less dense and much less viscous ($M \gg 1$). We take the viscosity of the slumping magma to be $10^{12}$ Pa s and the density difference, $\Delta\rho$ is 300 kgm$^{-3}$ (Sparks *et al.* [10]). This yields a timescale, $t_0$, of about twelve days. The volume of released magma is three cubic kilometers, which yields $V_0 \approx 1/2$. We found in section VI C that the late-time, unconfined approximation is accurate for times later than $T \sim 10^3$. This corresponds to 30 years, which is within the typical lifespan of a magma chamber. Finally, we consider the case in which new magma flows into the chamber with a constant flux of $q = 1$ m$^3$ s$^{-1}$ for which $\Lambda = 1.6\times10^{-4}$. The flow is dominated by buoyancy and is unconfined. The lubrication approximation is valid for $T \gg \Lambda^{-1/4}$, which corresponds to times much greater than three and a half months.

In future studies, it would be interesting to generalize the results to consider periodic input fluxes. Additionally, the extraction of the injected fluid would lead to different behavior and controls could be determined for when the current transitions from confined to unconfined in this context.

## DATA AVAILABILITY STATEMENT

The data that supports the findings of this study are available within the article.

## REFERENCES

[1] H. E. Huppert, "The propagation of two-dimensional and axisymmetric viscous gravity currents over a rigid horizontal surface," Journal of Fluid Mechanics **121**, 43–58 (1982).

[2]J. R. Lister, “Viscous flows down an inclined plane from point and line sources,” Journal of Fluid Mechanics **242**, 631–653 (1992).

[3]H. E. Huppert and A. W. Woods, “Gravity-driven flows in porous layers,” Journal of Fluid Mechanics **292**, 55–69 (1995).

[4]E. M. Hinton, A. J. Hogg, and H. E. Huppert, “Interaction of viscous free-surface flows with topography,” Journal of Fluid Mechanics **876**, 912–938 (2019).

[5]C. W. Sauer, “Mud displacement during cementing state of the art,” Journal of Petroleum Technology **39**, 1–091 (1987).

[6]E. B. Nelson and D. Guillot, “Well Cementing,” Developments in Petroleum Science (2006).

[7]S. M. Taghavi, T. Seon, D. M. Martinez, and I. A. Frigaard, “Buoyancy-dominated displacement flows in near-horizontal channels: the viscous limit,” Journal of Fluid Mechanics **639**, 1–35 (2009).

[8]S. S. Pegler, H. E. Huppert, and J. A. Neufeld, “Fluid injection into a confined porous layer,” Journal of Fluid Mechanics **745**, 592–620 (2014).

[9]E. M. Hinton and A. W. Woods, “Buoyancy-driven flow in a confined aquifer with a vertical gradient of permeability,” Journal of Fluid Mechanics **848**, 411–429 (2018).

[10]R. Sparks, C. Annen, J. Blundy, K. Cashman, A. Rust, and M. Jackson, “Formation and dynamics of magma reservoirs,” Philosophical Transactions of the Royal society A **377**, 20180019 (2019).

[11]P. A. Cole, K. Asteriadou, P. T. Robbins, E. G. Owen, G. A. Montague, and P. J. Fryer, “Comparison of cleaning of toothpaste from surfaces and pilot scale pipework,” Food and bioproducts processing **88**, 392–400 (2010).

[12]Z. Zheng, L. Rongy, and H. A. Stone, “Viscous fluid injection into a confined channel,” Physics of Fluids **27**, 062105 (2015).

[13]J. R. Lister and R. C. Kerr, “The propagation of two-dimensional and axisymmetric viscous gravity currents at a fluid interface,” Journal of Fluid Mechanics **203**, 215–249 (1989).

[14]P. Petitjeans and T. Maxworthy, “Miscible displacements in capillary tubes. Part 1. Experiments,” Journal of Fluid Mechanics **326**, 37–56 (1996).

[15]T. Seon, J.-P. Hulin, D. Salin, B. Perrin, and E. J. Hinch, “Buoyant mixing of miscible fluids in tilted tubes,” Physics of Fluids **16**, L103–L106 (2004).

[16]S. M. Taghavi, T. Seon, K. Wielage-Burchard, D. M. Martinez, and I. A. Frigaard, “Stationary residual layers in buoyant Newtonian displacement flows,” Physics of Fluids **23**, 044105 (2011).

[17]R. R. Kerswell, "Exchange flow of two immiscible fluids and the principle of maximum flux," Journal of Fluid Mechanics **682**, 132–159 (2011).

[18]G. P. Matson and A. J. Hogg, "Viscous exchange flows," Physics of Fluids **24**, 023102 (2012).

[19]A. Hasnain and K. Alba, "Buoyant displacement flow of immiscible fluids in inclined ducts: a theoretical approach," Physics of Fluids **29**, 052102 (2017).

[20]J. M. Nordbotten and M. A. Celia, "Similarity solutions for fluid injection into confined aquifers," Journal of Fluid Mechanics **561**, 307–327 (2006).

[21]M. A. Hesse, H. A. Tchelepi, B. J. Cantwel, and F. M. Orr, "Gravity currents in horizontal porous layers: transition from early to late self-similarity," Journal of Fluid Mechanics **577**, 363 (2007).

[22]Z. Zheng and J. A. Neufeld, "Self-similar dynamics of two-phase flows injected into a confined porous layer," Journal of Fluid Mechanics **877**, 882–921 (2019).

[23]H. E. Huppert, "Gravity currents: a personal perspective," Journal of Fluid Mechanics **554**, 299–322 (2006).

[24]S. M. Taghavi, "A two-layer model for buoyant displacement flows in a channel with wall slip," Journal of Fluid Mechanics **852**, 602–640 (2018).

[25]C. Pozrikidis, "Creeping flow in two-dimensional channels," Journal of Fluid Mechanics **180**, 495–514 (1987).

[26]M. Scholle, A. Wierschem, and N. Aksel, "Creeping films with vortices over strongly undulated bottoms," Acta Mechanica **168**, 167–193 (2004).

[27]B. Guo, Z. Zheng, M. A. Celia, and H. A. Stone, "Axisymmetric flows from fluid injection into a confined porous medium," Physics of Fluids **28** (2016).

[28]T. V. Ball, H. E. Huppert, J. R. Lister, and J. A. Neufeld, "The relaxation time for viscous and porous gravity currents following a change in flux," Journal of Fluid Mechanics **821**, 330–342 (2017).

[29]Y. Aboelkassem and A. E. Staples, "Flow transport in a microchannel induced by moving wall contractions: a novel micropumping mechanism," Acta Mechanica **223**, 463–480 (2012).

[30]P. Dudfield and A. W. Woods, "On the periodic injection of fluid into, and its extraction from, a porous medium for seasonal heat storage," Journal of Fluid Mechanics **707**, 467–481 (2012).

[31]P. G. Saffman and G. I. Taylor, "The penetration of a fluid into a porous medium or Hele-Shaw cell containing a more viscous liquid," Proceedings of the Royal Society of London. Series A. Mathematical and Physical Sciences **245**, 312–329 (1958).

[32]Z. Yang and Y. C. Yortsos, “Asymptotic solutions of miscible displacements in geometries of large aspect ratio,” Physics of Fluids **9**, 286–298 (1997).

[33]E. Lajeunesse, J. Martin, N. Rakotomalala, and D. Salin, “3D instability of miscible displacements in a Hele-Shaw cell,” Physical Review Letters **79**, 5254 (1997).

[34]I. Bischofberger, R. Ramachandran, and S. R. Nagel, “Fingering versus stability in the limit of zero interfacial tension,” Nature communications **5**, 1–6 (2014).

[35]Y. Liu, N. Balmforth, S. Hormozi, and D. Hewitt, “Two–dimensional viscoplastic dambreaks,” Journal of Non-Newtonian Fluid Mechanics **238**, 65–79 (2016).

[36]F. P. Bretherton, “The motion of long bubbles in tubes,” Journal of Fluid Mechanics **10**, 166–188 (1961).

[37]T. T. Al-Housseiny, P. A. Tsai, and H. A. Stone, “Control of interfacial instabilities using flow geometry,” Nature Physics **8**, 747–750 (2012).

[38]S. Li, J. S. Lowengrub, J. Fontana, and P. Palffy-Muhoray, “Control of viscous fingering patterns in a radial Hele-Shaw cell,” Physical Review Letters **102**, 174501 (2009).

[39]T. H. Beeson-Jones and A. W. Woods, “Control of viscous instability by variation of injection rate in a fluid with time-dependent rheology,” Journal of Fluid Mechanics **829**, 214–235 (2017).

[40]L. Paterson, “Fingering with miscible fluids in a Hele Shaw cell,” Physics of Fluids **1**, 26–30 (1985).

[41]K. N. Kowal and M. G. Worster, “Stability of lubricated viscous gravity currents. Part 2. Global analysis and stabilisation by buoyancy forces,” Journal of Fluid Mechanics **871**, 1007–1027 (2019).

[42]K. N. Kowal and M. G. Worster, “Lubricated viscous gravity currents,” Journal of Fluid Mechanics **766**, 626–655 (2015).

[43]K. N. Kowal and M. G. Worster, “Stability of lubricated viscous gravity currents. Part 1. Internal and frontal analyses and stabilisation by horizontal shear,” Journal of Fluid Mechanics **871**, 970–1006 (2019).

[44]H. E. Huppert, “Flow and instability of a viscous current down a slope,” Nature **300**, 427–429 (1982).

[45]J. S. Mathunjwa and A. J. Hogg, “Self-similar gravity currents in porous media: linear stability of the Barenblatt–Pattle solution revisited,” European Journal of Mechanics-B/Fluids **25**, 360–378 (2006).

[46]L. G. Leal, *Advanced Transport Phenomena: Fluid Mechanics and Convective Transport Processes*, Cambridge Series in Chemical Engineering No. 2 (Cambridge University Press, 2007).

[47]G. K. Batchelor, *An Introduction to Fluid Dynamics* (Cambridge university press, 1965).

[48]A. Kurganov and E. Tadmor, "New High-Resolution Central Schemes for Nonlinear Conservation Laws and Convection–Diffusion Equations," Journal of Computational Physics **160**, 241–282 (2000).

[49]Z. Zheng, B. Guo, I. C. Christov, M. A. Celia, and H. A. Stone, "Flow regimes for fluid injection into a confined porous medium," Journal of Fluid Mechanics **767**, 881–909 (2015).

[50]E. M. Hinton and A. W. Woods, "The effect of vertically varying permeability on tracer dispersion," J. Fluid Mech. **860**, 384–407 (2019).

[51]J. Ockendon, S. Howison, A. Lacey, and A. Movchan, *Applied Partial Differential Equations* (Oxford University Press, 2003).

[52]R. E. Pattle, "Diffusion From an Instantaneous Point Source With Concentration Dependent Coefficient," Quart. J. Mech. Appl. Math. **12**, 407–409 (1959).